



1 Dynamics of Variable Dusk-Dawn Flow Associated with Magnetotail 2 Current Sheet Flapping

3

4 James H. Lane¹, Adrian Grocott¹, Nathan A. Case¹, Maria-Theresia Walach¹

5

6 ¹ Department of Physics, Lancaster University, Lancaster, UK

7

8 Correspondence to: James Lane (j.lane@lancaster.ac.uk)

9

10

11 Abstract

12 Previous observations have provided a clear indication that the dusk-dawn (v_{ly}) sense of
 13 both slow ($< 200 \text{ km s}^{-1}$) and fast ($> 200 \text{ km s}^{-1}$) convective magnetotail flows is strongly
 14 governed by the Interplanetary Magnetic Field (IMF) B_y conditions. The related ‘untwisting
 15 hypothesis’ of magnetotail dynamics is commonly invoked to explain this dependence, in
 16 terms of a large-scale magnetospheric asymmetry. In the current study, we present Cluster
 17 spacecraft observations from 12 October 2006 of earthward convective magnetotail plasma
 18 flows whose dusk-dawn sense disagrees with the untwisting hypothesis of IMF B_y control of
 19 the magnetotail flows. During this interval, observations of the upstream solar wind
 20 conditions from OMNI, and ionospheric convection data using SuperDARN, indicate a large-
 21 scale magnetospheric morphology consistent with positive IMF B_y penetration into the
 22 magnetotail. Inspection of the in-situ Cluster magnetic field data reveals a flapping of the
 23 magnetotail current sheet; a phenomenon known to influence dusk-dawn flow. Results
 24 from the curlometer analysis technique suggest that the dusk-dawn flow perturbations may
 25 have been driven by the $\mathbf{J} \times \mathbf{B}$ force associated with a dawnward-propagating flapping of
 26 the magnetotail current sheet, locally overriding the expected IMF B_y control of the flows.
 27 We conclude that invocation of the untwisting hypothesis may be inappropriate when
 28 interpreting intervals of dynamic magnetotail behaviour such as during current sheet
 29 flapping.

30

31



32

33 1. Introduction

34

35 Convective magnetotail plasma flows at Earth, driven by the closing of magnetic flux via
 36 reconnection as part of the Dungey Cycle (Dungey, 1961) have been studied extensively for
 37 many years (e.g. Angelopoulos et al. 1992, 1994; Sergeev et al., 1996; Petrukovich et al.,
 38 2001; Cao et al., 2006; McPherron et al., 2011; Frühauff & Glassmeier, 2016). Arguably, the
 39 most well studied of these is the Bursty Bulk Flow (BBF). Angelopoulos et al. (1994) defined
 40 BBFs as being channels of earthward plasma flow continually above 100 km s^{-1} , exceeding
 41 400 km s^{-1} at one point across some interval, usually across a timescale of a few minutes.
 42 The flows are said to be the main transporter of mass, energy and flux in the magnetotail
 43 (e.g. Angelopoulos et al., 1994; Nakamura et al., 2002; Grocott et al., 2004a; Kiehas et al.,
 44 2018). Although their earthward nature is the key defining characteristic of BBFs, they will
 45 invariably exhibit a dusk-dawn component in their bulk flow as well (e.g. Angelopoulos et
 46 al., 1994; Petrukovich et al., 2001; Grocott et al., 2004b). Understanding the drivers of dusk-
 47 dawn asymmetries in magnetospheric dynamics is an important element of geospace
 48 research (e.g. Haaland et al., 2017).

49

50 A key factor that has been observed to influence the dusk-dawn direction of the
 51 magnetotail flow is the B_y component of the Interplanetary Magnetic Field (IMF). It is well
 52 established that when the IMF reconnects with the dayside terrestrial magnetic field, a non-
 53 zero IMF B_y component leads to asymmetric loading of open flux into the polar cap (e.g.
 54 Khurana et al., 1996; Tenfjord et al., 2015; Grocott et al., 2017; Ohma et al., 2019). This
 55 results in a twisting of the magnetotail whereby the closed field lines are rotated about the
 56 midnight meridian, and a B_y component is superimposed onto the tail field as a
 57 consequence of IMF B_y penetration (Cowley, 1981; Petrukovich, 2011; Tenfjord et al., 2015).
 58 Subsequently, following nightside reconnection, the tail will untwist (Grocott et al., 2004c),
 59 with the excitation of multiple convective flow bursts, each with an earthward and dusk-
 60 dawn component, in the tail and nightside ionosphere (Grocott et al., 2007). In order to be
 61 consistent with the tail ‘untwisting hypothesis’, any convective flows associated with an
 62 individual tail field line should share the same dusk-dawn direction (e.g. see Figure 3 of
 63 Grocott et al., 2005). The role of IMF B_y in the untwisting hypothesis has been examined



64 previously in a number of studies (e.g. Grocott et al, 2007; Pitkänen et al., 2013, 2015,
 65 2017). These studies revealed that under prolonged positive IMF B_y conditions, the
 66 earthward flows are expected to exhibit a dawnward component in the northern
 67 hemisphere ($B_x > 0$) and a duskward component in the southern hemisphere ($B_x < 0$), with
 68 the opposite correlation for negative IMF B_y conditions. IMF B_y has been shown to govern
 69 the dusk-dawn nature of these flows both during periods of steadier, slower convection
 70 (Pitkänen et al., 2019), as well as during more transient, dynamic BBF-like intervals (Grocott
 71 et al., 2007; Pitkänen et al., 2013). In the present study, we present observations of
 72 dawnward and duskward directed flows that do not match this expected dependence on
 73 IMF B_y , implying that the untwisting hypothesis is insufficient in this case. Instead, we
 74 suggest that the flows are being driven by local perturbations due to dynamic behaviour of
 75 the tail that are associated with flapping of the current sheet.

76
 77 The current sheet, or ‘neutral’ sheet, lies in the equatorial plane at the center of the tail
 78 plasma sheet and separates the earthward ($B_x > 0$) and tailward ($B_x < 0$) directed field (Ness,
 79 1965). The current sheet is a highly dynamic region of the Earth’s magnetotail which can
 80 undergo various types of net motion, such as tilting due to lobe magnetic pressures (Cowley
 81 et al., 1981; Tenfjord et al., 2017) as well as flapping. Flapping of the current sheet can
 82 generally be described as a sinusoidal-like variation in B_x of up to tens of nanoTesla, where
 83 an observing spacecraft often measures repeated changes in the sign of B_x (e.g. Runov et al.,
 84 2009), indicative of crossings of the current sheet, with characteristic times ranging from a
 85 few seconds to (more commonly) several minutes (e.g. Runov et al., 2009; Wu et al., 2016;
 86 Wei et al., 2019). Drivers of current sheet flapping have been widely investigated, with
 87 possible causes ranging from external solar wind/IMF changes (Runov et al., 2009),
 88 induction of hemispheric plasma asymmetries (Malova et al., 2007; Wei et al., 2015), fast
 89 earthward flow (Nakamura et al., 2009) as well as periodical, unsteady magnetotail
 90 reconnection (Wei et al., 2019). Studies such as Volwerk et al. (2008) and Kubyshkina et al.
 91 (2014) have illustrated that flapping of the current sheet can be associated with variable
 92 dusk-dawn flow, potentially overriding any IMF B_y control of the flow.

93
 94 In this paper we present Cluster spacecraft observations of an interval of dynamic
 95 magnetotail behaviour on 12 October 2006. Throughout this interval, Cluster 1 observed



oscillations in the magnetic field B_x component, which we attribute to current sheet flapping, concurrent with a series of convective fast flows with significant and variable dusk-dawn components. The B_y component of the concurrent upstream IMF had been largely positive for several hours prior to the flapping. Consequently, the interval discussed here provides an opportunity to investigate the possible competition of two distinct mechanisms for control of the dusk-dawn flow: 1) IMF B_y and 2) localized dynamics related to the flapping of the current sheet. In contrast to studies which have come before such as those presented by Grocott et al. (2007) and Pitkänen et al. (2015), the observed dusk-dawn direction of transient flow enhancements in this case disagrees with that which might be expected from the prevailing IMF B_y conditions, despite clear evidence for global penetration of positive IMF B_y . We therefore suggest that flapping of the current sheet had locally overridden the IMF B_y control of the dusk-dawn flow observed by Cluster 1.

2. Instrumentation and Data Sets

2.1. Spacecraft Data

The magnetospheric observations presented in this case study were made by the Cluster multi-spacecraft (C1-C4) constellation (Escoubet et al., 2001). We make use of the fluxgate magnetometer (FGM) onboard the Cluster spacecraft to obtain magnetic field measurements (Balogh et al., 2001), and obtain our bulk ion velocity data from the Hot Ion Analyser (HIA) on C1 and C3 calculated as on-board moments (Rème et al., 1997). The magnetic field data presented are 5 vectors-per-second (0.2s res) which have been 1s median-averaged, with the velocity data presented having spin resolution of just over 4s. Where these datasets have been combined to produce parameters such as the plasma beta and field-perpendicular velocities, we have resampled both the magnetic field and plasma data to 5s resolution. All data are presented in geocentric solar magnetospheric (GSM) coordinates unless stated otherwise.

The interval of study in this paper occurred between 00:00 – 00:55 UT on 12 October 2006. At 00:00 UT the Cluster spacecraft were located in the near-Earth magnetotail plasma sheet, in the pre-midnight sector. C1 was located at ($X = -14.7$, $Y = 6.0$, $Z = -1.2$) R_E , C2 at ($X = -14.2$, $Y = 7.5$, $Z = -0.7$) R_E , C3 at ($X = -13.9$, $Y = 7.0$, $Z = -2.1$) R_E , and C4 at ($X = -13.2$, $Y = 6.2$, $Z = -0.8$) R_E . This is depicted in Figure 1a by the colored triangles, along with the respective



spacecraft trajectories, from 00:00 – 00:55 UT, by the solid lines. Figure 1b shows a zoomed-out version of Figure 1a, which illustrates the location of the spacecraft with respect to the Earth. Figure 1b also shows a traced modelled magnetic field line, achieved using the semi-empirical TA15 model of the magnetosphere (Tsyganenko & Andreeva, 2015), which passes through the location of C1 and connects to both the northern and southern hemispheres of the Earth. We parameterised the TA15 model using mean-averaged solar wind dynamic pressure (P_{dyn}), IMF B_y and IMF B_z data from the 1-hour interval prior to 00:28 UT (the start of our specific interval of interest). These values were $P_{dyn} = 1.56$ nPa, IMF $B_y = +1.56$ nT and IMF $B_z = -2.17$ nT. There was also a tailward dipole tilt of $\approx -12^\circ$. The model was also parameterised with a solar wind coupling function index known as the ‘N index’, after Newell et al. (2007). The N index varies between 0 (quiet) and 2 (very active), and in this instance was ~ 0.4 .

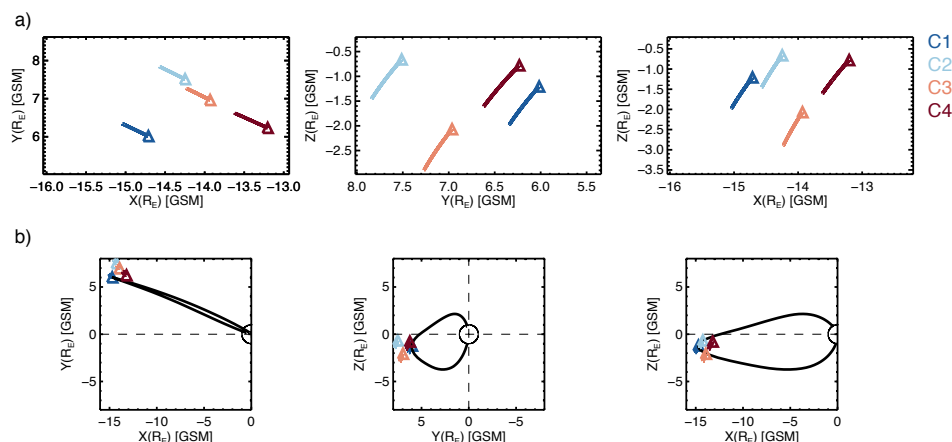


Figure 1: a) The locations of the Cluster spacecraft in the X-Y, Y-Z, and X-Z GSM planes, from left to right, respectively, at 00:00 UT on 12 October 2006, marked by the triangles. The trajectories from 00:00 UT to 00:55 UT are marked by the solid lines. The spacecraft are color-coded according to the key on the right. b) As in a), with a zoomed-out view. The Earth is shown by the solid circle. A TA15 model magnetic field line passing through the location of C1 is shown as the solid black line.



148 The IMF measurements used in this study were provided by the OMNIweb database at 1-
149 minute resolution, having been first propagated from L1 to the bow shock nose (King &
150 Papitashvili, 2005).

151

152 *2.2. SuperDARN Data*

153 The ionospheric observations presented in section 3.3 were provided by the Super Dual
154 Auroral Radar Network (SuperDARN), an international collaboration of 36 ground-based
155 radars (Nishitani et al., 2019) that make line-of-sight Doppler measurements of the
156 horizontal motion of the ionospheric plasma every few seconds (e.g. Chisham et al., 2007).
157 Here, we use 2-min ionospheric convection maps created by fitting the line-of-sight $\mathbf{E} \times \mathbf{B}$
158 velocity data to an eighth order expansion of the ionospheric electric potential in spherical
159 harmonics using the technique of Ruohoniemi & Baker (1998), implemented in the Radar
160 Software Toolkit (RST version 4.2, 2018). To accommodate intervals with limited data
161 availability, the data are supplemented with values derived from a statistical model
162 parameterized by IMF conditions. This is a well-established technique that has been
163 thoroughly discussed by, e.g., Chisham et al. (2007). The convection maps we present
164 employ the commonly used model of Ruohoniemi & Greenwald (1996). As a check on the
165 sensitivity of the maps to the choice of model input, we also tested the fitting using the
166 alternative model of Thomas and Shepherd (2018) and found that this has little impact on
167 the maps and no impact on our conclusions.

168

169 As a further measure to ensure that the choice of model is not critical to our results, we
170 chose not to use the concurrent IMF vector to parameterise the background model. In this
171 case, because we are using the SuperDARN data to provide evidence in support of the
172 expected large-scale influence of IMF B_y , we deemed it inappropriate to include model data
173 already parametrised by IMF B_y . We instead specify a nominal southward IMF with zero B_y
174 component in our analysis, to ensure that a background model with no pre-existing IMF B_y
175 influence is used. Although this might result in the patterns we show being less accurate
176 overall, especially in regions of poor data coverage, it will ensure that any B_y -associated
177 asymmetry in the maps is driven by the radar data from our interval of study, and not the
178 background model. This is discussed further in section 4.1, below.

179



180

181

182

183

184 **3 Observations**

185

186 In this section we present observations of the IMF, magnetotail magnetic field and plasma
187 flow, and ionospheric convection from an interval on 12 October 2006.

188

189 *3.1 IMF Observations*

190 Figure 2 presents an overview of the spacecraft data from an extended interval around our
191 period of specific interest for broader context. In Figure 2a, we show a time-series of the
192 IMF B_y and IMF B_z data from 20:00 UT on 11 October to 01:00 UT on 12 October 2006. These
193 data reveal that IMF B_y was generally positive for several hours prior to the fast flow
194 interval, with IMF B_z predominantly negative. There were three small intervals of negative
195 IMF B_y at $\sim 21:35$ UT, 23:00 UT and 23:40 UT and we discuss the possible ramifications of
196 these, and our treatment of them, in section 4.1.

197

198 *3.2 Cluster Spacecraft Observations*

199 In Figure 2b, we present the in-situ magnetic field and plasma measurements from the
200 Cluster spacecraft across the interval 00:00 – 00:55 UT.

201

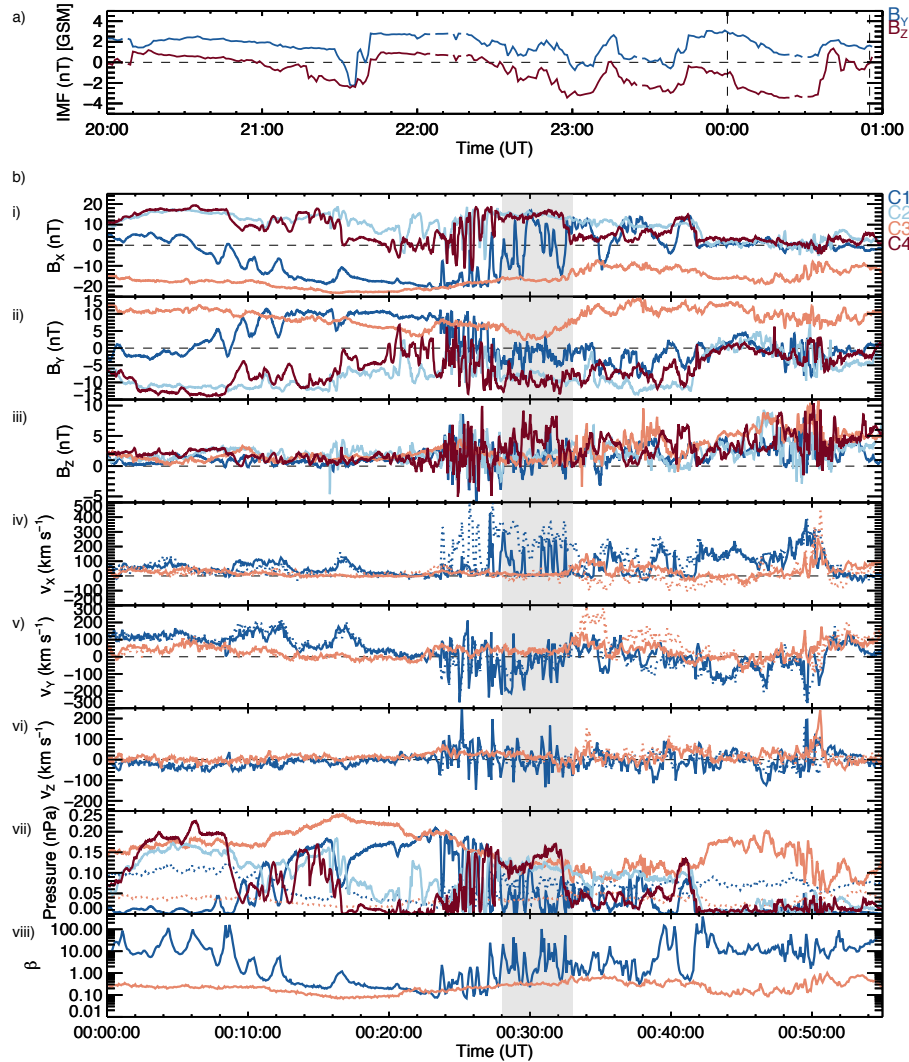


Figure 2: a) A plot of the IMF time series data for the IMF B_y (blue) and IMF B_z (red) components, from 20:00 UT on 11 October 2006 to 01:00 UT on 12 October 2006. The vertical dashed lines indicate the start (00:00 UT) and end (00:55 UT) of the interval of Cluster data (below). b) The in-situ Cluster spacecraft measurements. Shown first is the local magnetic field data, i) B_x , ii) B_y and iii) B_z , followed by the bulk ion velocity data, iv) v_x , v) v_y , and vi) v_z (dotted lines). The field-perpendicular component of the ion flow (indicative of the $\mathbf{E} \times \mathbf{B}$ convection) is shown in panels iv) to vi) by the solid lines. In panel vii) the magnetic $\left(\frac{B^2}{2\mu_0}\right)$ and thermal ion (nkT) pressures are shown by the solid and dotted lines respectively,



211 and in panel viii) the ion plasma beta from C1 and C3 is shown. All data are labelled
 212 according to the color-coded key on the right-hand side. The time-interval between the gray
 213 shaded region marks our specific interval of interest (discussed in text).

214

215

216 At ~00:06 UT, C1 crossed from the northern hemisphere into the southern hemisphere,
 217 illustrated by the sign change in B_x from positive to negative shown in Figure 2b i).
 218 Coincident with this, the observed B_y , shown in Figure 2b ii) turned from negative to
 219 positive. Figure 2b iv) reveals that up until ~00:24 UT, the earthward flow measured by both
 220 C1 and C3 was generally low in magnitude ($v_x < 100 \text{ km s}^{-1}$). The v_y component of the flow,
 221 shown in Figure 2b v), remained steadily duskward ($v_y > 0$) at C1 and duskward or close to
 222 zero at C3. The v_z component of the flow in Figure 2b vi), measured by C1 and C3 was
 223 effectively zero. During this period, the Cluster spacecraft that resided in the northern
 224 hemisphere (predominantly C2 and C4), observed $B_y < 0$, and the spacecraft which resided
 225 in the southern hemisphere (predominantly C1 and C3) observed $B_y > 0$. Occasionally a
 226 spacecraft encountered the current sheet ($B_x = 0$) at which point it observed $B_y = 0$. We
 227 comment on the significance of these magnetic field observations in section 4.2.

228

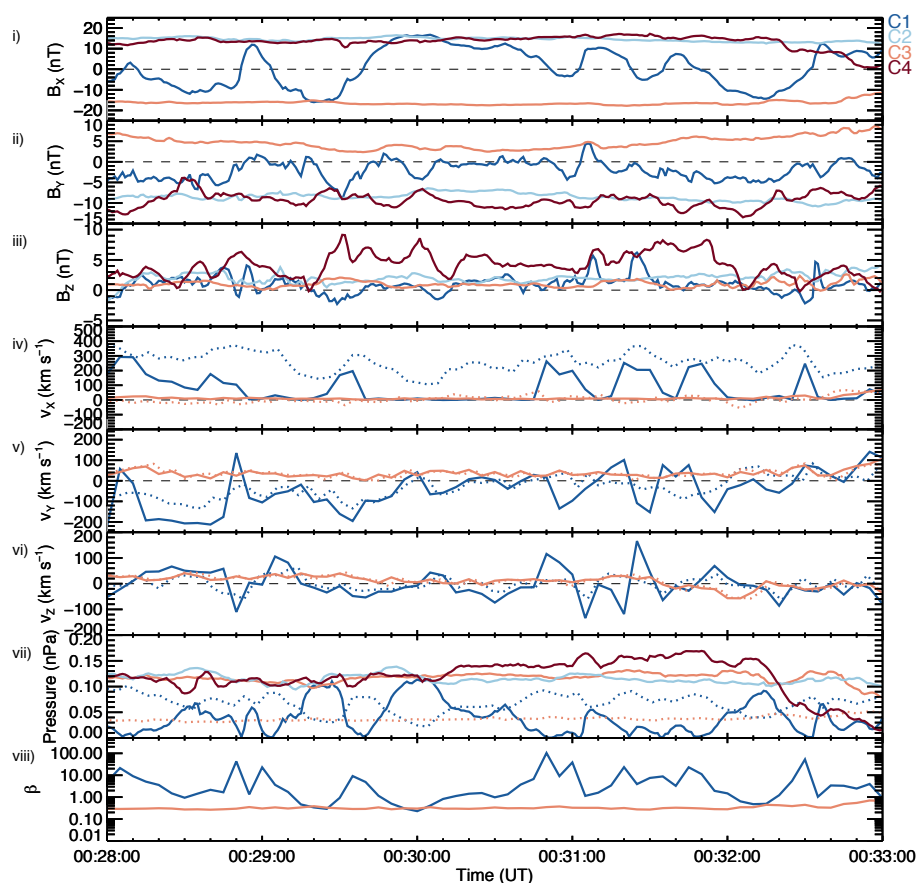
229 After ~00:24 UT, C1 began to observe a period of enhanced earthward flow
 230 ($v_x > 300 \text{ km s}^{-1}$) and variable dusk-dawn flow, concurrent with sudden variation in the local
 231 B_x component. Similarly, C2 and C4, but not C3, observed large magnitude ($> 20 \text{ nT}$) rapid
 232 variations in B_x , which appear to have an apparent timescale of around a minute and which
 233 we attribute to a flapping of the current sheet. As well as rapid variations in B_x , both the B_y
 234 and B_z components of C1, C2 and C4 seemed highly variable. As perhaps to be expected,
 235 these variations in the magnetic field were accompanied by significant variations in the
 236 magnetic pressure of ~0.15 nPa, as shown by the solid lines in Figure 2b vii).

237

238 Unlike the other spacecraft, C3 remained in the southern hemisphere throughout the entire
 239 interval and did not observe the rapid fluctuations in B_x . Between 00:28 – 00:33 UT (the gray
 240 shaded region), C1 began to repeatedly and rapidly cross the current sheet, as previously
 241 experienced by C2 and C4, whilst continually observing enhanced earthward flow and



242 variable dusk-dawn convective flow (v_{Ly}). Across the entire interval, the plasma beta, β ,
 243 indicated in Figure 2b viii), measured by C3 remained above ~ 0.1 , with C1's measured β
 244 ranging from 0.1 to over 100. This is consistent with the fact that C1 was continually
 245 crossing the current sheet at the center of the plasma sheet, where β is larger (Baumjohann
 246 et al., 1989). It is this interval of current sheet crossing and variable flow observed by C1
 247 that we focus on below and is presented in more detail in Figure 3.



248
 249 **Figure 3:** As in Figure 2b, but for the interval 00:28 – 00:33 UT on 12 October 2006.

250
 251 Figure 3 i) conveys the extent of the large-amplitude B_x variations observed by C1 between
 252 00:28 and 00:33 UT. B_x was generally fluctuating between positive and negative values
 253 throughout the five-minute interval, with a minimum at ~ -16 nT and maximum at ~ 17 nT.
 254 The magnetic pressure at C1 shown by the solid blue line in Figure 3 vii) is consistent with



the idea that C1 was crossing the current sheet, as this generally reached minima at the center of each current sheet crossing ($B_x \approx 0$). The B_y component (Fig. 3ii) measured by C1 generally remained negative and highly variable for the entire interval, with a number of large negative enhancements and a few small positive excursions. It is particularly of note that when C1 was below the neutral sheet, as implied by a negative B_x component, B_y was almost always negative. As we discuss in section 4.2, this is inconsistent with what we would expect based on the location of the spacecraft and also inconsistent with any expectation that a positive IMF B_y should have penetrated into the tail. The B_z component (Fig. 3iii) generally remained positive with some small negative excursions.

Unlike C1, C2-4 measured generally steady B_x throughout this five-minute period. C2 and C4 measured positive B_x , indicating that they were above the neutral sheet, and C3 measured negative B_x , indicating that it was below the neutral sheet. Similarly, B_y was steadily negative for C2 and C4 and steadily positive for C3. Again, we note the inconsistency between the C1 and C3 observations of B_y ; when in the southern hemisphere C1 generally observed $B_y < 0$, whereas C3 observed $B_y > 0$. On a few separate occasions C1 did briefly observe $B_y > 0$ (e.g. at 00:31:05 UT) but at these times C1 was located above the neutral sheet ($B_x > 0$), while C2 and C4 observed $B_y < 0$ above the neutral sheet. These variations in B_y imply the observation of a 'kink' in the field at the location of C1, the ramifications of which are discussed further in section 4.2.

At times when B_x observed by C1 was negative, indicating that C1 was below the neutral sheet, C1 generally observed negative (dawnward) $v_{\perp y}$ (Fig. 3v) with a magnitude varying between 100 and 200 km s⁻¹. At times when B_x became positive, indicating that C1 was above the neutral sheet, C1 tended to observe positive (duskward) $v_{\perp y}$, although this flow barely reached 100 km s⁻¹. The enhancements in $v_{\perp y}$ (both positive and negative) were generally accompanied by negative enhancements in B_y . Across the interval, there was a near continual $v_x > 200$ km s⁻¹ flow (blue dotted line in Fig. 3iv), peaking at almost 400 km s⁻¹, with concurrent peaks in the convective $v_{\perp x}$ component (solid blue line) of at least 200 km s⁻¹. The convective flow measured by C3, however, was generally very weak ($|v_{\perp}| < 50$ km s⁻¹) throughout this period (solid orange line in Fig 3iv). v_z (Fig. 3vi), as measured by



286 both C1 and C3 remained low in magnitude ($< 100 \text{ km s}^{-1}$) for the duration of the interval,
287 with a few $v_{\perp z}$ excursions above 100 km s^{-1} observed by C1. The most significant
288 enhancements in $v_{\perp z}$ seen by C1 appeared to occur in conjunction with the rapid current
289 sheet crossings between 00:30:50 and 00:32:00 UT. We discuss the implications of these
290 observations in the context of the upstream IMF conditions and large-scale magnetospheric
291 morphology in section 4.

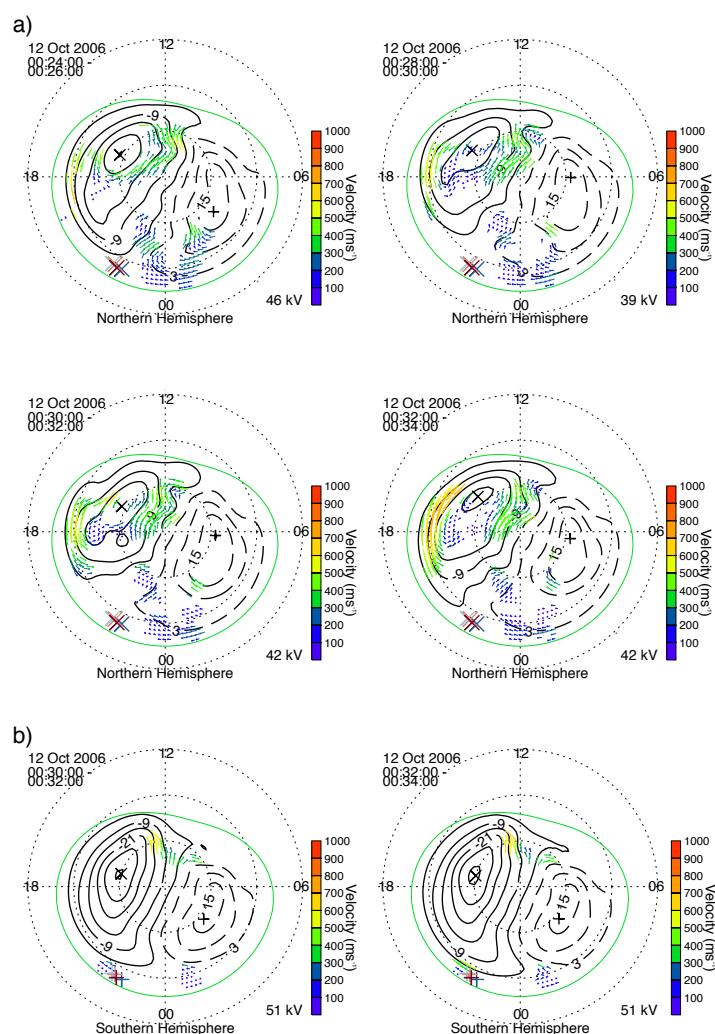
292

293

294 *3.3 Ionospheric Convection Observations*

295

296 To provide the large-scale context in which we can interpret the more localized
297 observations from the Cluster spacecraft we show ionospheric convection observations in
298 Figure 4. In Figure 4a we present a series of four 2-minute integration SuperDARN maps of
299 the northern hemisphere ionospheric convection pattern, beginning at 00:24 UT, and
300 ending at 00:34 UT, which encompasses our specific interval. In all maps, plasma is flowing
301 anti-sunward across the polar cap at high latitudes, also with a strong duskward sense, with
302 the direction of the convection reversing in the pre-midnight sector before returning
303 sunward at lower latitudes.



304

305 **Figure 4:** Maps of the ionospheric plasma convection derived from SuperDARN

306 observations. Midnight is to the bottom of each map, noon to the top, dusk to the left and

307 dawn to the right. The solid and dashed black lines represent the plasma streamlines and

308 are the contours of the electrostatic potential. Flow vectors are plotted at the locations of

309 radar observations and these are color-coded based on the magnitude of their velocity. a)

310 Four 2-minute northern hemisphere maps from 00:24 – 00:26, 00:28 – 00:30, 00:30 – 00:32

311 and 00:32 – 00:34 UT, respectively. b) Two 2-minute southern hemisphere maps from 00:30

312 – 00:32 and 00:32 – 00:34 UT, respectively. On each northern (southern) hemisphere map,



the footpoints of the Cluster spacecraft constellation are shown by the X's (+s), mapped using the TA15 model.

315

316

Owing to the coupled nature of the magnetosphere-ionosphere system, the observed ionospheric convection pattern is indicative of the global-scale magnetospheric convection (Cowley, 1981). In this case, the typical symmetrical twin-cell convection pattern has been rotated clockwise, with the dawn cell extending across into the pre-midnight sector, indicative of convection that has been driven under the influence of a positive IMF B_y component (e.g. Reistad et al., 2016, 2018). On each northern hemisphere map, the footpoints of the Cluster spacecraft constellation are indicated by the crosses (X), mapped using the TA15 model with the same parameterisation described in section 2.

325

Figure 4b shows two 2-minute integration SuperDARN maps of the southern hemisphere ionospheric convection pattern, beginning at 00:30 UT, and ending at 00:34 UT. The associated footpoints of the Cluster spacecraft are indicated by the plus signs (+). Although the coverage of radar data is much less than in the northern hemisphere, there are data in the pre- and post-midnight sectors which appears to be influencing the location of the flow reversal region at the nightside end of the dusk cell. Opposite to the northern hemisphere case, it is the dusk cell in the south which is extending towards, or just beyond, the midnight meridian. This is also consistent with a large-scale positive IMF B_y influence, owing to the expected north-south asymmetry of the influence of IMF B_y in the magnetosphere (e.g. Pettigrew et al., 2010). The significance of these observations is further discussed in section 4.1.

337

4. Analysis and Discussion

339

We have presented observations of a dynamic interval of plasma flows and magnetic field in the Earth's magnetotail. In this section we discuss our rationale for interpreting the flows as being inconsistent with large-scale magnetotail untwisting and our interpretation of their relationship to current sheet flapping.

344



345 4.1 Evidence for an inconsistency with large-scale magnetotail untwisting

346 During the five-minute interval studied (00:28 – 00:33 UT) C1 measured a continually
 347 fluctuating B_x component (Fig. 3i), indicative of multiple crossings of the tail current sheet.
 348 C1 was the only spacecraft to measure this signature across the interval (although similar
 349 signatures had been observed a few minutes earlier by C2 and C4). C1 also measured a
 350 series of earthward convective magnetotail fast flows with varying dusk-dawn components.
 351 The data in Figure 3 i) and Figure 3 v) illustrate that when B_x was positive (negative), a
 352 duskward (dawnward) $v_{\perp y}$ was generally observed. Additionally, the data in Figure 3 ii)
 353 show that C1 tended to observe a negative B_y component. According to the magnetotail
 354 untwisting hypothesis (e.g. Pitkänen et al., 2015), these flow and magnetic field
 355 observations are consistent with a negative IMF B_y penetration. The IMF data presented in
 356 Figure 2a, on the other hand, revealed that IMF B_y was generally positive for several hours
 357 prior to the fast flow interval (00:28 – 00:33 UT). Based on the IMF data alone, therefore,
 358 one might expect that a positive IMF B_y will have penetrated into the magnetosphere and
 359 thus ought to have determined the “expected” dusk-dawn direction of the flow. In that
 360 case, the flows observed here would have a dusk-dawn sense that is not explained by
 361 current theoretical models of magnetotail untwisting (e.g. Grocott et al., 2007). There are a
 362 number of possible explanations for this discrepancy and we address each one in turn.

363
 364 The first possibility is that our conclusion regarding what is the expected dusk-dawn
 365 asymmetry is incorrect. We noted in section 3.1 that there were three small negative IMF B_y
 366 excursions prior to our Cluster observations interval. Although the propagation of the IMF to
 367 the bow shock is accounted for in the OMNI data, there is uncertainty regarding the time it
 368 takes for the IMF B_y to ‘propagate’ into the magnetotail. Uncertainties in IMF B_y propagation
 369 times (e.g. Case & Wild, 2012) have previously been cited as an explanation for observing an
 370 unexpected asymmetry (e.g. Pitkänen et al., 2013). Studies such as Tenfjord et al. (2015,
 371 2017) and Case et al. (2018), for example, have suggested a reconfiguration time (to the
 372 prevailing IMF B_y conditions) for nightside closed field lines of around 40 minutes. At ~00:28
 373 UT (the beginning of our specific interval of interest), the IMF B_y had been positive for
 374 around 50 minutes. Based on the Tenfjord timescale, this would thus imply that our interval
 375 was wholly IMF $B_y > 0$ driven. Other studies, on the other hand, such as Browett et al.
 376 (2017), have shown that longer timescales of a few hours may be important.



377

378 However, for such long timescales to play a role one would expect to have observed a
379 relatively persistent IMF B_y component during that time. The integrated IMF B_y over the
380 hours prior to our interval was certainly convincingly B_y -positive, and it seems highly unlikely
381 that a few minute-long fluctuations into the opposite IMF B_y polarity, 1 or 2 hours prior to
382 the flows we observed, could have a significant influence. We can thus be confident that
383 positive IMF B_y was governing the global magnetospheric dynamics in this case.

384

385 Despite this convincing argument that the IMF data alone imply a positive IMF B_y
386 penetration, we performed an additional analysis to further ensure that these negative
387 excursions did not lead to a change in the global nature of the magnetosphere-ionosphere
388 system. We inspected the concurrent northern hemisphere SuperDARN data (presented in
389 Figure 4a) to provide evidence of the large-scale convection pattern. If the large-scale flow is
390 consistent with a positive IMF B_y component, then the magnetotail flows that we observed
391 must be deviating from this for some reason. The SuperDARN data indeed confirm that the
392 large-scale morphology of the system was consistent with a positive IMF B_y component (e.g.
393 Lockwood 1993; Grocott et al., 2017; Reistad et al., 2018). This can be inferred from the
394 general shape of the convection pattern, whereby across multiple maps (00:24 – 00:34 UT)
395 the pattern was rotated clockwise, with the dawn cell having extended into the pre-
396 midnight sector. That this is the expected convection pattern for an IMF B_y -driven
397 magnetosphere is also supported by the concurrent low level of geomagnetic activity. The
398 auroral AU and AL indices (not shown) confirm that this interval is geomagnetically quiet
399 (AU and |AL| both less than (or of the order of) 10 nT), such that the nightside ionospheric
400 convection asymmetry should be driven by IMF B_y rather than conductivity-driven features
401 such as the Harang discontinuity which might otherwise complicate the auroral zone flows
402 (e.g. Grocott et al., 2007; Grocott et al., 2008; Reistad et al., 2018).

403

404 The validity of the convection observations is further supported by the coverage of nightside
405 data which were used to constrain the model convection pattern. The data used to create a
406 SuperDARN convection map are supplemented by data from a statistical model (in this case
407 Ruohoniemi & Greenwald, 1996) which is typically parameterised by the instantaneous IMF
408 conditions. In the case that there is a lack of real data coverage, a created SuperDARN map



will be strongly influenced by the model data, as opposed to real data, and thus would reflect a prediction of convection based on the IMF conditions. The maps shown in Figure 4a illustrate that there were dozens of SuperDARN vectors in the midnight sector which were fitted to create the global convection maps. To confirm that these data were sufficient, and that the observed large-scale convection pattern was not being driven by model data, we parameterised the model in our analysis with IMF $B_y = 0$. Despite this, a clear IMF B_y -asymmetry exists, thus demonstrating that the observed large-scale IMF $B_y > 0$ global convection patterns must be data-driven.

A second possible explanation for the discrepancy between the dusk-dawn direction of the local and global-scale convection concerns the certainty with which we can determine the location of the spacecraft with respect to the large-scale convection pattern. The untwisting hypothesis relies on the assumption that the convection cell to which the spacecraft is connected should be a factor of only hemisphere and the sense of IMF B_y (e.g. Pitkänen et al., 2013, 2017). In other words, as discussed above, for $B_y > 0$, the hypothesis dictates that C1 ought to be located on the dawn cell when above the neutral sheet and the dusk cell when below, at least in the case that the spacecraft is close to midnight (Grocott et al., 2007). This might be true statistically, but it is not clear how valid an assumption it might be when trying to interpret observations from a single event in the presence of a highly dynamic neutral sheet. It also fails to account for the dusk-dawn location of the spacecraft, which in this case was $6 \lesssim Y \lesssim 7 R_E$. If, as a result, the spacecraft was actually located on the dusk cell when above the neutral sheet, and on the dawn cell when below the neutral sheet, then the sense of the observed plasma sheet flows would actually be consistent with the large-scale convection.

One way to specify which cell the spacecraft is located within is to map its location into the ionosphere. This has been done using TA15 and is shown by the crosses (X) on the northern hemisphere convection maps and by plus signs (+) on the southern hemisphere convection maps, in Figures 4a and 4b, respectively. This mapping suggests that the assumption above is correct.



440 Consider first the northern hemisphere map from 00:30 – 00:32 UT in Figure 4a: the
441 spacecraft map close to the dawn cell, such that the duskward flow that C1 observed there
442 would seem to be inconsistent. However, it is worth considering that the pre-midnight
443 location of the spacecraft, the proximity of the mapped footpoints to the dusk cell, and the
444 level of uncertainty generally accepted to be present in field line mapping, may give
445 credence to the possibility that the spacecraft actually mapped to the dusk cell in the
446 northern hemisphere. If this was the case, then the northern hemisphere flows observed by
447 C1 would actually be consistent with the large-scale convection pattern. However, if we
448 consider the southern hemisphere maps in Figure 4b we can be more certain of which cell
449 the spacecraft map to. Owing to the IMF B_y positive nature of the convection (i.e. the more
450 extended southern hemisphere dusk cell) and the pre-midnight location of the spacecraft,
451 the footpoints are located quite convincingly on the dusk cell. This is despite the dusk-dawn
452 asymmetry being less pronounced than that seen in the northern hemisphere (and the
453 associated poorer coverage of southern hemisphere SuperDARN data). When below the
454 neutral sheet C1 observed downward flows, meaning it would have to have been on the
455 southern hemisphere dawn cell to be consistent with the large-scale convection, which is
456 clearly not the case. It seems much more likely, therefore, that C1 observed flow that was
457 associated with localized magnetic field dynamics rather than being a signature of the large-
458 scale convection.

459

460 *4.2 Evidence for a local perturbation in the magnetotail*

461 The lack of consistency with the large-scale convection leads us to a third explanation for
462 our observations, which is that there is a local perturbation within the tail that is
463 independent of any large-scale, IMF B_y -controlled asymmetry associated with magnetotail
464 untwisting. This is supported by the observations from the other Cluster spacecraft. The
465 low-level of flow seen by C3 is mostly duskward (Fig. 3v) and therefore consistent with the
466 idea of untwisting under IMF $B_y > 0$, given its southern hemisphere location. Further, in
467 Figure 2b v), up until the rapid B_x variations began at ~00:24 UT, fast duskward flow in the
468 southern hemisphere was also seen by C1. The fact that C3 continued to then observe
469 steady duskward flow, and no significant B_x change, suggests that the change in the nature
470 of the C1 observations after 00:24 UT must in-fact be due to some localized process that

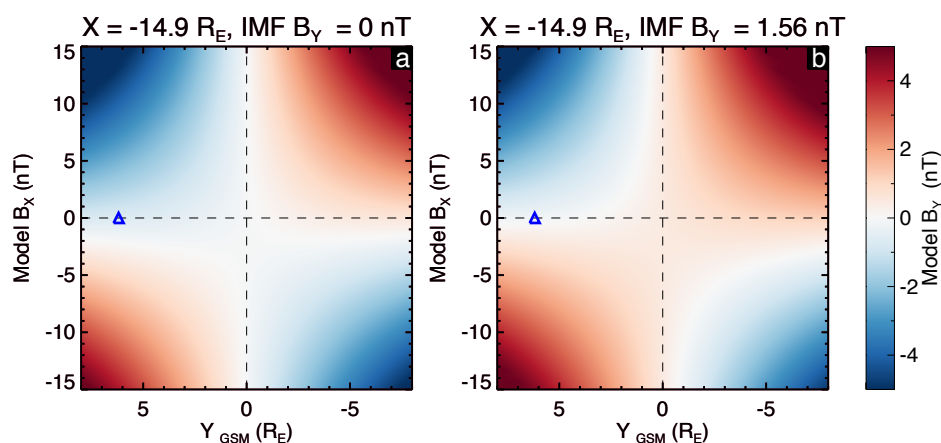


471 was responsible for driving the downward component of the flows which was only observed
 472 by C1.

473

474 This idea of a local perturbation is also supported by the variations in the local B_y
 475 component. Figure 3 ii) illustrates the in-situ variations in B_y with time across the interval.
 476 Despite there clearly being positive IMF B_y penetration globally (as confirmed by inspection
 477 of the OMNI and SuperDARN data), C1, C2 and C4 all recorded mostly negative local B_y
 478 values. In the studies of, e.g., Pitkänen et al. (2013, 2017) this observation would have been
 479 offered as evidence of a negative of IMF B_y penetration, thus supporting the untwisting
 480 hypothesis. However, it is important to note that a negative local B_y component may be
 481 wholly consistent with positive IMF B_y . There are, in fact, multiple sources of B_y in the tail,
 482 such as magnetotail flaring (Fairfield, 1979), as well as tilt effects and current sheet warping
 483 (see e.g. Petrukovich et al., 2005), in addition to a penetration of the IMF B_y . To fully
 484 interpret the magnetic field observations, we must therefore consider the possible effects
 485 of these phenomena on the presence of B_y in the tail at the specific location of each
 486 spacecraft.

487



488

489 **Figure 5:** TA15 model magnetic field data. In each case, plotted is Y vs B_x [GSM], (at
 490 $X = -14.9 R_E$, i.e. the X position of C1 at ~00:28 UT on 12 Oct 2006), with the TA15 modelled
 491 B_y value shown by the color bar on the right. The blue triangle shows the Y -location of C1, at
 492 $B_x = 0$. In panel (a) we have imposed IMF $B_y = 0$, and for panel (b) we have used the 1-hour
 493 mean-averaged IMF B_y (+1.56 nT) in the hour prior to 00:28 UT.



494

495 To aid in this interpretation, we present TA15 model magnetic field data in Figure 5, to
 496 provide an indication of the expected background B_y -component at the time of our interval.
 497 These data, from $X = -14.9 R_E$, are plotted against Y [GSM]-position on the horizontal axis,
 498 and against the B_x -component on the vertical axis. We have reversed the conventional
 499 direction of the horizontal axis (negative to positive from left to right) to be consistent with
 500 a view looking earthward from downtail. In panel (a) we show the field for the case that IMF
 501 $B_y = 0$ and in panel (b) the case that IMF $B_y = +1.56$ nT (the 1-hour mean-averaged IMF B_y in
 502 the hour prior to 00:28 UT). The first conclusion we can make from consideration of the B_y
 503 component in Figure 5a is how, even under no IMF B_y penetration, a ‘background’ B_y value
 504 will exist in the tail purely dependent on location. In such a ‘symmetric’ tail, one would
 505 expect the background B_y value to appear as one moves away from midnight toward the
 506 dusk-dawn flanks, as well as further above and below the neutral sheet. Pre-midnight, we
 507 would expect to observe negative B_y above the neutral sheet ($B_x > 0$), and positive B_y below
 508 the neutral sheet ($B_x < 0$), with the opposite effect post-midnight. This is the effect known as
 509 magnetotail flaring (Fairfield, 1979).

510

511 The data in Figure 5a also show the effect of the negative (tailward) dipole tilt (as
 512 appropriate to our study interval) and current sheet warping on the local B_y component.
 513 According to Petrukovich (2011) the current sheet warping (controlled by the dipole tilt) is
 514 expected to add a negative B_y component pre-midnight and a positive B_y component post-
 515 midnight. Furthermore, the ‘even tilt’ effect is expected to add a negative B_y component to
 516 both the pre and post-midnight sectors for a negative tilt. This leads to the effect seen in
 517 Figure 5a where in the pre-midnight sector, the location of the B_y polarity change occurs in
 518 the southern hemisphere (at $B_x \approx -3$ nT).

519

520 Figure 5b illustrates the scenario relevant to our case study, where we have additionally a
 521 global positive IMF B_y penetration. This additional positive B_y has the effect of moving the
 522 location of the pre-midnight B_y polarity change back up towards the neutral sheet. This
 523 explains why the Cluster spacecraft observed $B_y \approx 0$ when $B_x \approx 0$ during the few tens of
 524 minutes prior to our interval, as noted in section 3.2. This also explains why C2-3 and C4
 525 observed the polarity of B_y that they did throughout the interval. It is thus clear that positive



IMF B_y penetration does not mean we should expect to observe positive B_y everywhere in the tail, rather, it simply means that there is expected to be some positive B_y perturbation to the already present ‘background’ B_y at a particular location. As Figure 5b demonstrates, C2 and C4 (located above the neutral sheet) are expected to have observed negative B_y even though positive IMF B_y has penetrated into the magnetotail. The background B_y expected at their location (pre-midnight, $B_x > 0$), is negative and the IMF B_y -associated perturbation was not large enough to enforce a sign change in B_y .

The Cluster spacecraft in our study were all located pre-midnight (+Y GSM). From Figure 3, C2 and C4 observed positive B_x , and negative B_y , and at ~00:28 UT were located at around $Z = -1 R_E$ (Figure 1). C3, however, observed negative B_x and positive B_y , and was located at around $Z = -2.5 R_E$. The location of the neutral sheet crossing at ~00:28 UT can therefore be said (locally) to have been somewhere between -1 and $-2.5 R_E$ in Z . C1 was located at around $Z = -1.5 R_E$ and, throughout the five-minute interval, observed a B_x which continually fluctuated from positive to negative, yet observed mostly weakly negative B_y . For B_y to have remained negative, despite C1 moving above and below the neutral sheet, suggests that there was a B_y negative ‘kink’ in the magnetotail that was localized to the vicinity of C1. This is further supported by the fact that numerous (albeit brief) positive B_y excursions occurred when C1 was above the neutral sheet (as noted in section 3.2). We use the term ‘kink’ to highlight a deformation in the nearby field lines which results in the observed perturbations to the local B_y component. We suggest that this deformation could be relatively small in terms of field line length, much like a kink in a cable or wire. In the following section, we investigate this kink in relation to the observed current sheet flapping.

549
 550

4.3 Evidence for current sheet flapping as a source of the asymmetric flows

If a localized magnetic field perturbation was associated with the lack of observation of the expected dusk-dawn flow for magnetotail untwisting, investigating its cause seems a worthwhile endeavour. The clear sinusoidal-like variation in B_x observed by C1, which is evidence of current sheet flapping (e.g. Runov et al., 2009), provides us with a starting point for this investigation. This flapping must be highly localized as at the time of our five-minute flow interval (00:28 -00:33 UT), only C1 observed the flapping. MVA analysis (Sonnerup &



558 Cahill, 1967) suggests that the flapping was a kink-like wave which was propagating
 559 downward (Rong et al., 2015; Wu et al., 2016), and therefore may have been a source of the
 560 observed dusk-dawn flow.

561

562 The causes of current sheet flapping have been discussed previously (Runov et al., 2009;
 563 Wei et al., 2019). One such cause has been attributed to localized, periodical reconnection –
 564 a process known to drive Bursty Bulk Flows (BBFs) in the magnetotail (Angelopoulos et al.,
 565 1994; Zhang et al., 2016). In fact, BBFs excited directly as a result of reconnection in the tail
 566 have been previously linked to magnetic fluctuations in the current sheet (Nakamura et al.,
 567 2009; Wu et al., 2016). Examining the data presented in Figure 3 iii) and Figure 3 iv), we
 568 note that C1 measured a generally positive B_z , with a few negative blips, as well as
 569 continually fast ($v_x > 200 \text{ km s}^{-1}$) earthward flow, peaking at over 370 km s^{-1} with bursts of
 570 enhanced convective flow ($v_{\perp x} > 200 \text{ km s}^{-1}$) also apparent. These observations are fairly
 571 consistent with (if slightly slower than) the original definition of a BBF (Angelopoulos et al.,
 572 1994). This, along with the absence of similar flow observations in the C3 data, suggests that
 573 C1 may have been located earthward of a localized reconnection site (owing to $B_z > 0$),
 574 where persistent, localized reconnection was exciting fast earthward flow. The reconnection
 575 process may then have been driving the current sheet flapping, inducing the localized kink in
 576 the field, and ultimately controlling the dusk-dawn direction of the convective flow.

577

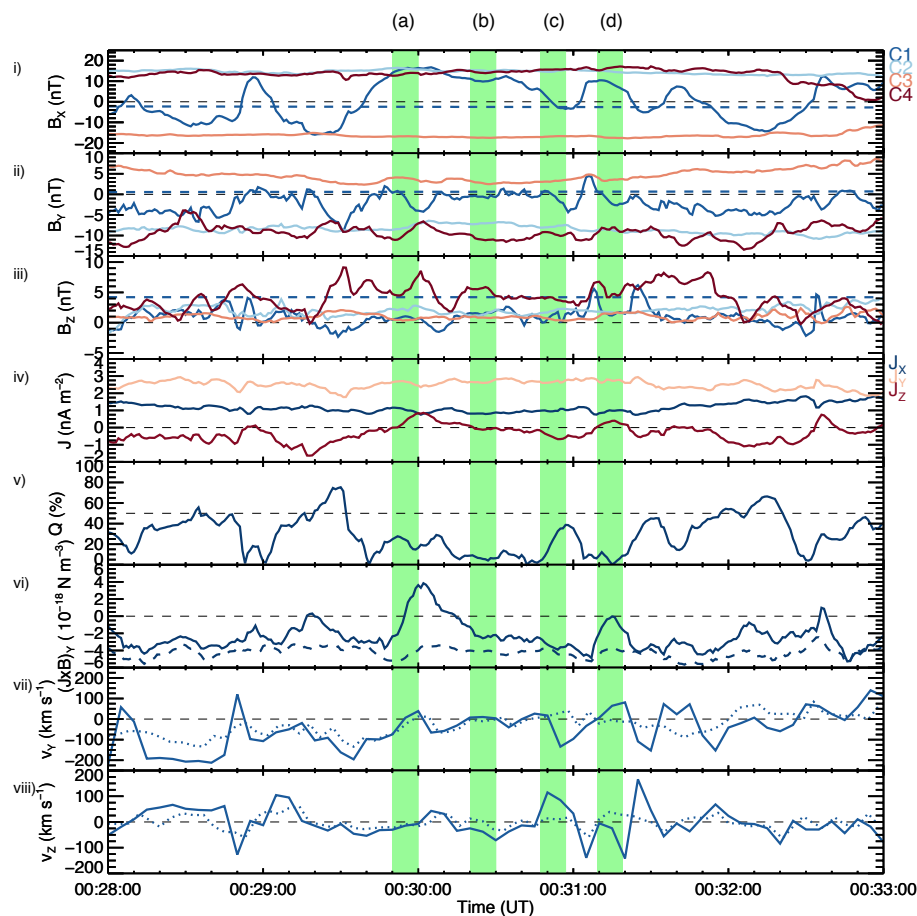
578

579 It is well known that the magnetic tension force is responsible for the acceleration of plasma
 580 following reconnection (Karlsson et al., 2015). Our observations of a dusk-dawn flow
 581 component may be related to the localized magnetic tension forces driving and directing
 582 plasma flows in association with the flapping. In order to provide some scope to this
 583 suggestion, we attempted to find the direction of the $\mathbf{J} \times \mathbf{B}$ forces acting on the plasma. We
 584 used the curlometer technique (Dunlop et al., 1988, 2002), to estimate the average current
 585 density, \mathbf{J} , flowing through the volume bound by the spacecraft tetrahedron. The $\mathbf{J} \times \mathbf{B}$
 586 force density [N m^{-3}] is then calculated by taking the cross product of \mathbf{J} with the average
 587 magnetic field vector \mathbf{B} from the four-spacecraft (Karlsson et al., 2015).

588



589 In order to check the validity of using the curlometer approach, we calculated the quality
 590 parameter, Q , defined as $|\nabla \cdot \mathbf{B}|/|\nabla \times \mathbf{B}|$. It is generally accepted that a value of $Q < 0.5$ is
 591 required for a current estimate to be valid. Hence, the value of Q , along with due
 592 consideration of the spacecraft configuration and its orientation relative to the magnetic
 593 field structure, may be used as a monitor of how reliable the curlometer approach is
 594 (Dunlop et al., 2002). This is discussed further below, in reference to the analysis shown in
 595 Figure 6.
 596



597
 598 **Figure 6:** i-iii) The local magnetic field vector \mathbf{B} (B_x , B_y , B_z) observed by C1-4, as shown
 599 previously (solid lines) and the TA15 modelled \mathbf{B} vector for C1 (dashed blue lines). iv) The
 600 components of the current density vector \mathbf{J} (J_x , J_y , J_z), v) Q , vi) $(\mathbf{J} \times \mathbf{B})_y$ (solid blue line) and $(\mathbf{J}$



601 $\times \mathbf{B})_y$ computed using the TA15 modelled C1 \mathbf{B} (dashed line, discussed in-text), vii) v_y ($v_{\perp y}$
 602 in solid lines), observed by C1 and viii) v_z ($v_{\perp z}$ in solid lines), also observed by C1. The green
 603 highlighted regions labelled (a), (b), (c) and (d) correspond to four specific time-windows of
 604 interest (discussed in-text).

605

606 Shown in Figure 6 i-iii) are the local magnetic field B_x , B_y and B_z components, as presented
 607 previously. In Figure 6 iv) are the current density J_x , J_y and J_z components determined from
 608 the curlometer analysis. In Figure 6 vi) is the dusk-dawn component of $\mathbf{J} \times \mathbf{B}$. In panels i-iii)
 609 and vi), also shown is a dashed blue line. In panels (i-iii) this represents the TA15 modelled
 610 magnetic field (see section 4.2) at the location of C1. In panel (vi) this represents the $(\mathbf{J} \times \mathbf{B})_y$
 611 force where \mathbf{J} and the average \mathbf{B} have been computed using the model field at the location
 612 of C1 and the true magnetic fields measured by C2-C4, hereafter referred to as the ‘model (\mathbf{J}
 613 $\times \mathbf{B})_y$ force’. This has been computed to provide an illustration of what one would expect
 614 the ‘unperturbed’ magnetic field of C1 and the associated $(\mathbf{J} \times \mathbf{B})_y$ force to look like, in the
 615 absence of any dynamical effects such as current sheet flapping or field line ‘kinking’. Figure
 616 6 v) suggests that our curlometer approach is generally appropriate, as Q mostly remains
 617 below 50% (horizontal dashed line) for the five-minute interval. We note that, unlike in
 618 previous studies which have used the curlometer technique at inter-spacecraft separation
 619 distances of $\ll 1 R_E$ (e.g. Dunlop et al., 2002; Runov et al., 2003), in our case the Cluster
 620 spacecraft separation is large ($\gtrsim 1 R_E$). Therefore, the curlometer is likely to be an
 621 underestimate of the true current at these scale sizes. Critically, however, the spacecraft
 622 configuration is such that the estimate of the direction of the currents should be stable.
 623 Thus, although the volume enclosed by the spacecraft is greater than the scale sizes of the
 624 current sheet flapping and kink, a reliable estimate of the direction of the net $\mathbf{J} \times \mathbf{B}$ force
 625 within the enclosed volume may still be obtained.

626

627 Two key features of Figure 6 are apparent. Firstly, it appears as though the perturbations to
 628 $(\mathbf{J} \times \mathbf{B})_y$, displayed in Figure 6 vi), are associated with the magnetic field perturbations
 629 generally only observed by C1. Second, the downward flow bursts (reproduced in Fig. 6 vii)
 630 tend to occur when $(\mathbf{J} \times \mathbf{B})_y$ is more negative, with the weak duskward flow bursts occurring



631 when $(\mathbf{J} \times \mathbf{B})_y$ is less negative. We note that there is not a one-to-one correlation between
 632 the $(\mathbf{J} \times \mathbf{B})_y$ and $v_{\perp y}$ data. This could well be due to the large volume over which $\mathbf{J} \times \mathbf{B}$ is
 633 being averaged and we make no attempt to interpret the detailed variations in $(\mathbf{J} \times \mathbf{B})_y$
 634 implied by these data. However, as this region of space will contain the localized flapping
 635 and kink, the calculated $\mathbf{J} \times \mathbf{B}$ should be influenced by these dynamics and hence still
 636 provide an indication of the forces acting within that region. The consistency between the
 637 direction of $(\mathbf{J} \times \mathbf{B})_y$ and $v_{\perp y}$ therefore suggests that the $\mathbf{J} \times \mathbf{B}$ force associated with the
 638 current sheet flapping is exerting some level of control over the direction of the convective
 639 flow. We also note that the $(\mathbf{J} \times \mathbf{B})_y$ force is effectively always less negative than the model
 640 $(\mathbf{J} \times \mathbf{B})_y$ force. As can be seen in Figure 6 vi), the model $(\mathbf{J} \times \mathbf{B})_y$ force is acting steadily
 641 downward, consistent with the duskward location of the spacecraft and suggesting that the
 642 curlometer analysis is simply picking up the $(\mathbf{J} \times \mathbf{B})_y$ force associated with the ‘background
 643 curvature’ of the magnetic field. Thus, we suggest that the positive deviations of $(\mathbf{J} \times \mathbf{B})_y$
 644 from the model $(\mathbf{J} \times \mathbf{B})_y$ force are due to the perturbations (flapping and kinking) observed
 645 by C1.

646

647

648

649 *4.4 Visualization of the observed dynamics*

650 In an effort to visualize these plasma sheet dynamics, we show in Figure 7 a series of
 651 sketches that attempt to associate the observed magnetic field perturbations with the
 652 observed dusk-dawn convective flows. The panels correspond to the four time windows
 653 indicated on Figure 6 by the highlighted regions labelled a-d. In each panel, we indicate the
 654 approximate relative position of the 4 Cluster spacecraft in GSM coordinates, and the
 655 appropriate sense of B_y measured by each spacecraft is shown by the purple arrows at each
 656 spacecraft location (the Z-component of the field was in fact generally small, and has been
 657 exaggerated here for illustrative purposes). We also superimpose nominal plasma sheet
 658 field lines (again with an exaggerated extent in Z) that display the sense of B_y implied by the
 659 TA15 data presented in Figure 5 (long blue curved arrows). The dashed lines represent the
 660 location of the neutral sheet at the end of each time window. This is tilted slightly, as



appropriate for IMF $B_y > 0$, but with the end-state of the “flap” of the current sheet implied by the sign of B_x observed by C1. In red is the perturbation to the field implied by the sign of B_y observed by C1.

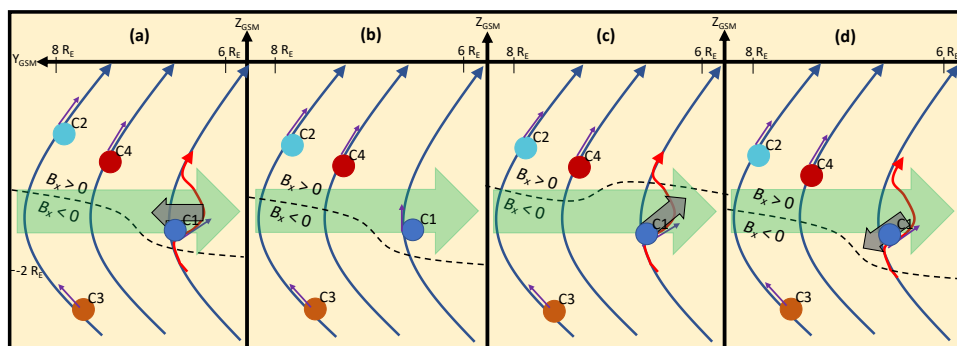


Figure 7: Schematic diagrams of the observed magnetic field perturbations and dusk-dawn convective flows during the time-windows indicated in Fig. 6 by the highlighted regions. The approximate locations of the four Cluster spacecraft relative to one-another in the Y-Z GSM plane are indicated (not to scale) by the colored circles. The curved blue arrows represent magnetic field lines, and the short purple arrow indicates the local sense of B_y at the location of each spacecraft. The dashed black line indicates the current sheet. In panels (a), (b) and (d), the curved red arrow shows the ‘kinked’ magnetic field line. The long thick green arrow shows the direction of the model $(\mathbf{J} \times \mathbf{B})_y$ force associated with the background curvature of the magnetic field, and the small thick gray arrow shows the direction of the dusk-dawn convective flow observed by C1.

In Figure 7a C1 is located above the current sheet and measured negative B_y . A weakly duskward convective flow was observed at this time (as indicated by the thick gray arrow), consistent with the duskward sense of the $(\mathbf{J} \times \mathbf{B})_y$ force, and opposite to the sense of the model $(\mathbf{J} \times \mathbf{B})_y$ force associated with the background curvature of the magnetic field. In Figure 7b, C1 is still above the current sheet but measured $B_y \approx 0$ and no dusk-dawn convective flow. In Figure 7c C1 is shown below the current sheet, where the background B_y would be positive (see Fig 5b). C1 instead observed an increasingly negative B_y , which we



685 suggest is associated with the presence of the kink in the field. At the same time, C1 also
 686 observed a convective plasma flow with downward and slightly upward (+Z) component
 687 (thick gray arrow). We therefore suggest that the flow was associated with the
 688 upward/dawnward flap of the current sheet, and that the downward sense of the flow likely
 689 also resulted in the increase in negative B_y seen during the time-window shown in Figure 6c.
 690 In Figure 7d C1 is shown above the current sheet, where it observed a weakly negative B_y . In
 691 this case, C1 observed a convective plasma flow with duskward and slightly downward (–Z)
 692 component. Similarly to in Figure 7a, this flow occurred in concert with a positive
 693 enhancement in $(\mathbf{J} \times \mathbf{B})_y$ relative to the model $(\mathbf{J} \times \mathbf{B})_y$. This flow would therefore seem to
 694 be associated with the downward flap of the current sheet, and its duskward sense could
 695 indicate that it is acting to reduce the negative kink in B_y that is apparent over the time-
 696 window shown in Figure 6d.

697

698 Whilst we acknowledge a degree of uncertainty in the details of the interpretation
 699 presented above of the specific relationship between the flows and the field, it serves to
 700 illustrate three observations about this interval of which we can be very certain: 1) The IMF,
 701 ionospheric convection, and plasma sheet magnetic field observations all lead to the
 702 expectation of an IMF $B_y > 0$ large-scale asymmetry in the magnetosphere. 2) The Cluster 1
 703 spacecraft observed convective flow with a dusk-dawn component that was inconsistent
 704 with current theories of IMF B_y -induced dusk-dawn flows associated with magnetotail
 705 untwisting. We therefore note that the observations presented here cannot be attributed to
 706 the current model of large-scale magnetotail untwisting. 3) Magnetic field perturbations
 707 that were indicative of a localized current sheet flapping and dusk-dawn kink in the field
 708 occurred coincident with the flows. It therefore seems likely that IMF B_y -driven asymmetries
 709 are not the only mechanism by which a dusk-dawn component may be introduced into the
 710 convective flow, with other dynamical processes also likely to contribute.

711

712

713

714

715



716 5. Summary

717

718 We have presented a case study from 12 October 2006 revealing a dynamic interval of
 719 plasma flows and current sheet flapping, observed by the Cluster 1 spacecraft. The key
 720 observations presented in this study may be summarised as follows:

721

- 722 • The OMNI data revealed that the IMF B_y had been positive for several hours prior to
 723 our interval of Cluster data, with the exception of three short-lived negative
 724 excursions.
- 725 • The SuperDARN ionospheric convection observations revealed a large-scale
 726 asymmetry consistent with IMF $B_y > 0$.
- 727 • C1 observed a changing B_x magnetic field component, and associated duskward ($v_{\perp y}$
 728 > 0) flow when in the northern magnetic hemisphere, and dawnward ($v_{\perp y} < 0$) flow
 729 in the southern magnetic hemisphere.

730

731 Contrary to the results of a number of previous studies in the literature, during this
 732 particular interval, the dusk-dawn sense of the convective magnetotail flows ($v_{\perp y}$) does not
 733 agree with expectations based on the theoretical understanding of global magnetotail
 734 untwisting and the prevailing positive IMF B_y conditions. We instead attribute the flows to a
 735 localized magnetic field perturbation, or ‘kink’ in the magnetotail, which appeared to be
 736 independent of any large-scale IMF B_y controlled asymmetry and may have been related to
 737 the observed current sheet flapping. We attributed the current sheet flapping to being
 738 driven by localized reconnection, itself inferred from the presence of the observed bursty
 739 fast earthward flow ($v_{\perp x} \approx 200 \text{ km s}^{-1}$). Analysis using the curlometer technique suggests
 740 that the $\mathbf{J} \times \mathbf{B}$ force associated with the current sheet flapping could have been exerting a
 741 level of control over the convective flow responsible for introducing the observed dusk-
 742 dawn component.

743

744 Whilst it is known that variable dusk-dawn flow can occur in conjunction with current sheet
 745 flapping, this case study has provided direct evidence that flapping can locally override the
 746 expected IMF B_y control of dusk-dawn magnetotail flow, in spite of clear global penetration



of IMF $B_y > 0$; consequently, resulting in the production of localized flows that do not agree with the expected direction for global magnetotail untwisting. Further studies by the authors are currently underway to determine if this is a frequent occurrence, and to consider, and account for, localized tail dynamics more fully in a statistical analysis of the magnetotail flows.

Acknowledgements

The authors would like to thank the FGM and CIS teams as part of the Cluster mission and acknowledge the Cluster Science Archive (Laakso et al., 2010) as the source of the Cluster data. We also wish to thank the OMNIWeb as the source of the solar wind and IMF data. The authors acknowledge the use of SuperDARN data. SuperDARN is a collection of radars funded by national scientific funding agencies of Australia, Canada, China, France, Japan, South Africa, United Kingdom, and United States of America, and we thank the international PI team for providing the data. The authors acknowledge access to the SuperDARN database via BAS data mirror (<http://bslsuperdarn.ncrc-bas.ac.uk:8093/docs/>) and are grateful for use of the Radar Software Toolkit (RST v4.2 <https://zenodo.org/record/1403226#.Xy0u7y3MxTY>) with which the raw radar data were processed. We acknowledge the WDC for Geomagnetism, Kyoto, for use of the auroral electrojet indices, which may be obtained from <http://wdc.kugi.kyoto-u.ac.jp/aedir/>. We are also grateful to Haje Korth for providing the IDL Geopack DLM containing the Tsyganenko magnetic field model routines and coordinate system conversions and wish to thank Nikolai Tsyganenko for useful discussion of his magnetic field models. Finally, we are thankful for the advice of Malcolm Dunlop regarding the applicability of the curlometer technique at large spacecraft separations. This research was undertaken with the support of funding from the following sources: Lancaster University Faculty of Science and Technology studentship (JHL), STFC Consolidated grant no. ST/R000816/1 (NAC, AG), NERC standard grant nos. NE/P001556/1 and NE/T000937/1 (MTW, AG).

References

- Angelopoulos, V., Baumjohann, W., Kennel, C. F., Coroniti, F. V., Kivelson, M. G., Pellat, R., Walker, R. J., Lühr, H. and Paschmann, G. (1992). Bursty bulk flows in the inner central plasma sheet. *J. Geophys. Res.*, 97 (A4), 4027-4039. doi:10.1029/91JA02701
- Angelopoulos, V., Kennel, C. F., Coroniti, F. V., Pellat, R., Kivelson, M. G., Walker, R. J., Russell, C. T., Baumjohann, W., Feldman W. C. and Gosling, J. T. (1994). Statistical characteristics of bursty bulk flow events. *J. Geophys. Res.*, 99 (A11), 21,257-21,280. doi:10.1029/94JA01263
- Balogh, A., Carr, C. M., Acuña, M. H., Dunlop, M. W., Beek, T. J., Brown, P., Fornaçon, K. -H., Georgescu, E., Glassmeier, K. -H., Harris, J., Musmann, G., Oddy, T. and Scwingenschuh, K. (2001). The Cluster magnetic field investigation: Overview of in-flight performance and initial results. *Ann. Geophys.*, 19, 1207-1217. doi: 10.5194/angeo-19-1207-2001



- 791
 792 Baumjohann, W., Paschmann, G. and Cattell, C. A. (1989). Average Properties in the Central
 793 Plasma Sheet. *Journal of Geophysical Research*, 94 (A6), 6597-6606. doi:
 794 10.1029/JA094iA06p06597
 795
 796 Browett, S. D., Fear, R. C., Grocott, A., and Milan, S. E. (2017). Timescales for the penetration
 797 of IMF B_y into the Earth's magnetotail. *J. Geophys. Res.: Space Physics*, 122 (1), 579-593.
 798 doi:10.1002/2016JA023198
 799
 800 Cao, J. B., Ma, Y. D., Parks, G., Rème, H., Dandouras, I., Nakamura, R., Zhang, T. L., Zong, Q.,
 801 Lucek, E., Carr, C. M., Liu, Z. X. and Zhou, G. C. (2006). Joint observations by Cluster satellites
 802 of bursty bulk flows in the magnetotail. *J. Geophys. Res.*, 111 (A4), A04206.
 803 doi:10.1029/2005JA011322
 804
 805 Case, N. A., Grocott, A., Haaland, S., Martin, C. J., and Nagai, T. (2018). Response of the
 806 Earth's Neutral Sheet to Reversals in the IMF B_y component. *J. Geophys. Res.*, 123 (10),
 807 8206-8218. doi:10.1029/2018JA025712
 808
 809 Case, N. A. and Wild, J. (2012). A statistical comparison of solar wind propagation delays
 810 derived from multispacecraft techniques. *J. Geophys. Res.*, 117 (A2), A02101,
 811 doi:10.1029/2011JA016946.
 812
 813 Chisham G., Lester, M., Milan, S. E., Freeman, M. P., Bristow, W. A., Grocott A., McWilliams,
 814 K. A., Ruohoniemi, J. M., Yeoman, T. K., Dyson, P. L., Greenwald, R. A., Kikuchi, T., Pinnock,
 815 M., Rash, J. P. S., Sato, N., Sofko, G. J., Villain, J. -P. and Walker, A. D. M. et al. (2007). A
 816 decade of the Super Dual Auroral Radar Network (SuperDARN): scientific achievements,
 817 new techniques and future directions. *Surveys in Geophysics* 28, 33-109.
 818 doi:10.1007/s10712-007-9017-8
 819
 820 Cowley, S. W. H. (1981). Magnetospheric asymmetries associated with the y -component of
 821 the IMF. *Planet Space Sci*, 29 (1), 79-96. doi:10.1016/0032-0633(81)90141-0
 822
 823 Dungey, J. W. (1961). Interplanetary magnetic field and the auroral zones. *Phys. Rev. Lett.*, 6,
 824 47-48. doi:10.1103/PhysRevLett.6.47
 825
 826 Dunlop, M. W., Southwood, D. J., Glassmeier, K. -H., and Neubauer, F. M. (1988). Analysis of
 827 multipoint magnetometer data. *Advances in Space Research*, 8 (9-10), 273-277.
 828 doi:10.1016/0273-1177(88)90141-X
 829
 830 Dunlop, M. W., Balogh, A., Glassmeier, K. -H. and Robert, P. (2002). Four-point Cluster
 831 application of magnetic field analysis tools: The Curlometer. *J. Geophys. Res.*, 107 (A11).
 832 doi:10.1029/2001JA005088
 833
 834 Escoubet, C. P., Fehringer, M. and Goldstein, M. (2001). The Cluster Mission. *Ann. Geophys.*,
 835 19, 1197 – 1200. doi:10.5194/angeo-19-1197-2001
 836



- 837 Fairfield, D. H. (1979). On the Average Configuration Of The Geomagnetic Tail. *J. Geophys.*
 838 *Res.*, 84 (A5), 1950-1958. doi:10.1029/JA084iA05p01950
- 839
- 840 Frühauff, D. and Glassmeier, K.-H. (2016). Statistical analysis of magnetotail fast flows and
 841 related magnetic disturbances. *Ann. Geophys.*, 34, 399-409. doi:10.5194/angeo-34-399-
 842 2016
- 843
- 844 Grocott, A. (2017). Time Dependence of Dawn-Dusk Asymmetries in the Terrestrial
 845 Ionospheric Convection Pattern. In: Haaland, S. et al. (2017), *Dawn-Dusk Asymmetries in*
 846 *Planetary Plasma Environments*, John Wiley and Sons, Inc., 107-123
- 847
- 848 Grocott, A., Yeoman, T. K., Nakamura, R., Cowley, S. W. H, Frey, H. U., Rème, H. and Klecker,
 849 B. J. (2004a). Multi-instrument observations of the ionospheric counterpart of a bursty bulk
 850 flow in the near-Earth plasma sheet. *Ann. Geophys.*, 22, 1061-1075, 1432-0576/ag/2004-22-
 851 1061.
- 852
- 853 Grocott, A., Yeoman, T. K., Cowley, S. W. H, and Rème, H. (2004b). Multi-instrument
 854 observations of bursty bulk flows and their ionospheric counterparts. *Proc. Seventh Internat.*
 855 *Conf. on Substorms*, UDK-52-854, FMI, Helsinki, Finland, 107-110.
- 856
- 857 Grocott, A., Badman, S. V., Cowley, S. W. H, and Cripps (2004c). The influence of the IMF B_y
 858 on the nature of the nightside high-latitude ionospheric flow during intervals of positive IMF
 859 B_z . *Ann. Geophys.*, 22, 1755-1764, doi:10.5194/angeo-22-1755-2004.
- 860
- 861 Grocott, A., Yeoman, T. K., Milan, S. E. and Cowley, S. W. H. (2005), Interhemispheric
 862 observations of the ionospheric signature of tail reconnection during IMF-northward non-
 863 substorm intervals, *Ann. Geophys.*, 23, 1763–1770. doi:10.5194/angeo-23-1763-2005.
- 864
- 865 Grocott, A., Yeoman, T. K., Milan, S. E., Amm, O., Frey, H. U., Juusola, L., Nakamura, R.,
 866 Owen, C. J., Rème, H. and Takada, T. (2007). Multi-scale observations of magnetotail flux
 867 transport during IMF-northward non-substorm intervals. *Ann. Geophys.*, 25, 1709-1720.
 868 doi:10.5194/angeo-25-1709-2007
- 869
- 870 Grocott, A., Milan, S. E. and Yeoman, T. K. (2008). Interplanetary magnetic field control of
 871 fast azimuthal flows in the nightside high-latitude ionosphere, *Geophys. Res. Lett.*, 35,
 872 L08102, doi:10.1029/2008GL033545.
- 873
- 874 Haaland, S., Runov, A. and Forsyth, C. (2017). Dawn-Dusk Asymmetries in Planetary Plasma
 875 Environments, *Geophysical Monograph 230, First Edition. American Geophysical Union.*
 876 Published 2017 by John Wiley & Sons, Inc.
- 877
- 878 Karlsson, T., Hamrin, M., Nilsson, H., Kullen, A., and Pitkänen, T. (2015). Magnetic forces
 879 associated with bursty bulk flows in the Earth's magnetotail. *Geophys. Res. Lett.*, 42 (9),
 880 3122-3128. doi:10.1002/2015GL063999
- 881



- 882 Kiehas, S. A., Runov, A., Angelopoulos, V., Hietala, H. and Korovinskiy, D. (2018). Magnetotail
 883 Fast Flow Occurrence Rate and Dawn-Dusk Asymmetry at $X_{GSM} \sim -60 R_E$. *J. Geophys. Res.:*
 884 *Space Physics*, 123 (3), 1767 – 1778. doi:10.1002/2017JA024776
- 885
 886 King, J. H., and Papitashvili, N. E. (2005). Solar wind spatial scales in and comparisons of
 887 hourly Wind and ACE plasma and magnetic field data. *J. Geophys. Res.*, 110, A02104.
 888 doi:10.1029/2004JA010649
- 889
 890 Khurana, K. K., Walker, R. J., and Ogino, T. (1996). Magnetospheric convection in the
 891 presence of interplanetary magnetic field By: A conceptual model and simulations, *J.*
 892 *Geophys. Res.*, 101 (A3), 4907–4916. doi:10.1029/95JA03673
- 893
 894 Kubyshkina, D. I., Sormakov, D. A., Sergeev, V. A., Semenov, V. S., Erkaev, N. V., Kubyshkin, I.
 895 V., Ganushkina, N. Yu. And Dubyagin, S. V. (2014). How to distinguish between kink and
 896 sausage modes in flapping oscillations? *J. Geophys. Res.*, 119, 3,002-3,015.
 897 doi:10.1002/2013JA019477.
- 898
 899 Laakso, H., C. Perry, S. McCaffrey, D. Herment, A.J. Allen, C.C. Harvey, C.P. Escoubet, C.
 900 Gruenberger, M.G.G.T. Taylor, and R. Turner (2010), Cluster Active Archive: Overview, 3-37,
 901 The Cluster Active Archive, Astrophysics and Space Science Proceedings, H. Laakso et al.
 902 (eds.), Springer.
- 903
 904 Lockwood, M. (1993), Modelling high-latitude ionosphere for time-varying plasma
 905 convection, IEE Proceedings-H, Vol. 140. No. 2. doi:10.1049/ip-h-2.1993.0015
- 906
 907 Malova, H. V., Zelenyi, L. M., Popov, V. Y., Petrukovich, A. A. and Runov, A. V. (2007).
 908 Asymmetric thin current sheets in the Earth's magnetotail. *Geophys. Res. Lett.*, 34 (16),
 909 L16108. doi:10.1029/2007GL030011
- 910
 911 McPherron, R. L., Hsu, T. -S., Kissinger, J., Chu, X., and Angelopoulos, V., (2011).
 912 Characteristics of plasma flows at the inner edge of the plasma sheet. *J. Geophys. Res.*, 116
 913 (A5), A00133. doi:10.1029/2010JA015923
- 914
 915 Nakamura, R., Baumjohann, W., Klecker, B., Bogdanova, Y., Balogh, A., Rème, H., Bosqued, J.
 916 M., Dandouras, I., Sauvaud, J. A., Glassmeier, K. -H., Kistler, L., Mouikis, C., Zhang, T. L.,
 917 Eichelberger, H. and Runov, A. (2002). Motion of the dipolarization front during a flow burst
 918 event observed by Cluster. *Geophys. Res. Lett.*, 29 (20), 1942. doi:/10.1029/2002GL015763
- 919
 920 Nakamura, R., Retinò, A., Baumjohann, W., Volwerk, M., Erkaev, N., Klecker, B., Lucek, E. A.,
 921 Dandouras, I., André, M. and Khotyainstev, Y. (2009). Evolution of dipolarization in the near-
 922 Earth current sheet induced by Earthward rapid flux transport. *Ann. Geophys.*, 27, 1743-
 923 1754. doi:10.5194/angeo-27-1743-2009
- 924
 925 Ness, N. F. (1965). The Earth's Magnetic Tail. *J. Geophys. Res.*, 70 (13), 2989–3005.
 926 doi:10.1029/JZ070i013p02989
- 927



- 928 Newell, P. T., Sotirelis, T., Liou, K., Meng, C. -I. and Rich, F. J. (2007). A nearly universal solar
 929 wind-magnetosphere coupling function inferred from 10 magnetospheric state variables. *J.*
 930 *Geophys. Res.*, **112** (A1), A01206. doi: 10.1029/2006JA012025
- 931
- 932 Nishitani, N., Ruohoniemi, J. M., Lester, M., Baker, J. B. H., Koustov, A. V., Shepherd, S. G.,
 933 Chisham, G., Hori, T., Thomas, E. G., Makarevich, R. A., Marchaudon, A., Ponomarenko, P.,
 934 Wild, J. A., Milan, S. E., Bristow, W. A., Devlin, J., Miller, E., Greenwald, R. A., Ogawa, T. and
 935 Kikiuchi, T. (2019). Review of the accomplishments of mid-latitude Super Dual Auroral Radar
 936 Network (SuperDARN) HF radars. *Progress in Earth and Planetary Science*, **6**:27.
 937 doi:10.1186/s40645-019-0270-5
- 938
- 939 Ohma, A., Østgaard, N., Reistad, J. P., Tenfjord, P., Laundal, K. M., Moretto Jørgensen, T.,
 940 Haaland, S. E., Krcelic, P. and Milan, S. (2019). Observations of Asymmetric Lobe Convection
 941 for Weak and Strong Tail Activity. *J. Geophys. Res.: Space Physics*, **124** (12).
 942 doi:10.1029/2019JA026773
- 943
- 944 Pettigrew, E. D., Shepherd, S. G. and Ruohoniemi, J. M. (2010). Climatological patterns of
 945 high-latitude convection in the Northern and Southern hemispheres: Dipole tilt
 946 dependencies and interhemispheric comparisons. *J. Geophys. Res.*, **115**, doi:
 947 10.1029/2009JA014956.
- 948
- 949 Petrukovich, A. A. (2011). Origins of plasma sheet B_y . *J. Geophys. Res.*, **116** (A7), A07217.
 950 doi:10.1029/2010JA016386
- 951
- 952 Petrukovich, A. A., Baumjohann, W., Nakamura, R., Schödel, R., and Mukai, T. (2001). Are
 953 earthward bursty bulk flows convective or field-aligned? *J. Geophys. Res.*, **106** (A10), 21,211-
 954 21,215. doi:10.1029/2001JA900019
- 955
- 956 Petrukovich, A. A., Baumjohann, W., Nakamura, R., Runov, A., and Balogh, A. (2005). Cluster
 957 vision of the magnetotail current sheet on a macroscale. *J. Geophys. Res.*, **110** (A6), A06204.
 958 doi:10.1029/2004JA010825
- 959
- 960 Pitkänen, T., Hamrin, M., Norqvist, P., Karlsson, T., and Nilsson, H. (2013). IMF dependence
 961 of the azimuthal direction of earthward magnetotail fast flows. *Geophys. Res. Lett.*, **40** (21),
 962 5598-5604. doi:10.1002/2013GL058136
- 963
- 964 Pitkänen, T., Hamrin, M., Norqvist, P., Karlsson, T., Nilsson, H., Kullen, A., Imber, S. M. and
 965 Milan, S. E. (2015). Azimuthal velocity shear within an earthward fast flow: further evidence
 966 for magnetotail untwisting? *Ann. Geophys.*, **33**, 245-255. doi:10.5194/angeo-33-245-2015
- 967
- 968 Pitkänen, T., Hamrin, M., Karlsson, T., Nilsson, H., and Kullen, A. (2017). On IMF B_y -Induced
 969 Dawn-Dusk Asymmetries in Earthward Convective Fast Flows. In: Haaland, S. et al. (2017),
 970 *Dawn-Dusk Asymmetries in Planetary Plasma Environments*, John Wiley and Sons, Inc., 107-
 971 123.
- 972
- 973 Pitkänen, T., Kullen, A., Laundal, K. M., Tenfjord, P., Shi, Q. Q. Park, J. -S., Hamrin, M., De
 974 Spiegeleer, A., Chong, G. S. and Tian, A. M. (2019). IMF B_y Influence on Magnetospheric



- 975 Convection in Earth's Magnetotail Plasma Sheet. *Geophys. Res. Lett.*, **46** (21), 11,698-11,708.
 976 doi:10.1029/2019GL084190
 977
- 978 Reistad, J. P., Østgaard, N., Tenfjord, P., Laundal, K. M., Snekvik, K., Haaland, S., Milan, S. E.,
 979 Oksavik, K., Frey, H. U. and Grocott, A. (2016). Dynamic effects of restoring footprint
 980
- 981 Reistad, J. P., Østgaard, N., Laundal, K. M., Ohma, A., Snekvik, K., Tenfjord, P., Grocott, A.,
 982 Oksavik, K., Milan, S. E. and Haaland, S. (2018). Observations of asymmetries in ionospheric
 983 return flow during different levels of geomagnetic activity, *J. Geophys. Res.*, **123**.
 984 doi:10.1029/2017JA025051
 985
- 986 symmetry on closed magnetic field lines. *J. Geophys. Res.: Space Physics*, **121** (5),
 987 015JA022058. doi:10.1002/2015JA022058
 988
- 989 Rème, H., Bosqued, J. M., Sauvaud, J. A., Cros, A., Dandouras, J., Aoustin, C., Bouyssou, J.,
 990 Camus, Th., Cuvilo, J., Martz, C., Médale, J. L., Perrier, H., Romefort, D., Rouzaud, J., d'Uston,
 991 C., Möbius, E., Crocker, K., Granoff, M., Kistler, L. M., Popecki, M., Hovestadt, D., Klecker, B.,
 992 Paschmann, G., Scholer, M., Carlson, C. W., Curtis, D. W., Lin, R. P., McFadden, J. P.,
 993 Formisano, V., Amata, E., Bavassano-Cattaneo, M. B., Baldetti, P., Belluci, G., Bruno, R.,
 994 Chionchio, G., Di Lellis, A., Shelley, E. G., Ghielmetti, A. G., Lennartsson, W., Korth, A.,
 995 Rosenbauer, H., Lundin, R., Olsen, S., Parks, G. K., McCarthy, M. and Balsiger, H. (1997). The
 996 Cluster Ion Spectrometry (CIS) Experiment. *Space Sci. Rev.*, **79**, 303-350. doi:10.1007/978-
 997 94-011-5666-0_12
 998
- 999 Rong, Z. J., Barabash, S., Stenberg, G., Futaana, Y., Zhang, T. L., Wan, W. X., Wei, Y. and
 1000 Wang, X. -D. (2015). Technique for diagnosing the flapping motion of magnetotail current
 1001 sheets based on single-point magnetic field analysis. *J. Geophys. Res.: Space Physics*, **120** (5),
 1002 3462-3474. doi:10.1002/2014JA020973
 1003
- 1004 Runov, A., Nakamura, R., Baumjohann, W., Zhang, T. L., Volwerk, M., Eichelberger, H. -U. and
 1005 Balogh, A. (2003). Cluster observations of a bifurcated current sheet. *Geophys. Res. Lett.*, **30**
 1006 (2), 1036. doi:10.1029/2002GL016136
 1007
- 1008 Runov, A., Angelopoulos, V., Sergeev, V. A., Glassmeier, K. -H., Auster, U., McFadden, J.,
 1009 Larson, D. and Mann, I. (2009). Global properties of magnetotail current sheet flapping:
 1010 THEMIS perspectives. *Ann. Geophys.*, **27**, 319-328. doi:10.5194/angeo-27-319-2009
 1011
- 1012 Ruohoniemi, J. M. and Baker, K. B. (1998). Large-scale imaging of high-latitude convection
 1013 with Super Dual Auroral Radar Network HF radar observations. *J. Geophys. Res.*, **103** (A9),
 1014 20,797-20,811. doi:10.1029/98JA01288
 1015
- 1016 Ruohoniemi, J. M. and Greenwald, R. A. (1996). Statistical patterns of high-latitude
 1017 convection obtained from Goose Bay HF radar observations. *J. Geophys. Res.*, **101** (A10),
 1018 21,743-21,763. doi:10.1029/96JA01584
 1019



- 1020 Sergeev, V. A., Angelopoulos, V., Gosling, J. T., Cattell, C. A., and Russell, C. T. (1996).
 1021 Detection of localized, plasma-depleted flux tubes or bubbles in the midtail plasma sheet. *J.*
 1022 *Geophys. Res.*, *101* (A5), 10,817 – 10,826. doi:10.1029/96JA00460
 1023
- 1024 Sonnerup, B. U. Ö, and Cahill Jr, L. J. (1967). Magnetopause structure and attitude from
 1025 Explorer 12 observations. *J. Geophys. Res.*, *72* (1), 171-183.
 1026 doi:10.1029/JZ072i001p00171
 1027
- 1028 Sonnerup, B. U. Ö and Scheible, M. (1998). Minimum and Maximum Variance Analysis. In:
 1029 Paschmann, G. and Daly, W. (1998), *Analysis Methods for Multi-Spacecraft Data*, pp 185-
 1030 220, ESA Publications Division, Noordwijk, Netherlands.
 1031
- 1032 Tenfjord, P., Østgaard, N., Snekvik, K., Laundal, K. M., Reistad, J. P., Haaland, S., and Milan, S.
 1033 E. (2015). How the IMF B_y induces a B_y component in the closed magnetosphere and how it
 1034 leads to asymmetric currents and convection patterns in the two hemispheres. *J. Geophys.*
 1035 *Res.: Space Physics*, *120* (11), 9368-9384. doi:10.1002/2015JA021579
 1036
- 1037 Tenfjord, P., Østgaard, N., Strangeway, R., Haaland, S., Snekvik, K., Laundal, K. M., Reistad, J.
 1038 P. and Milan, S. E. (2017). Magnetospheric response and reconfiguration times following
 1039 IMF B_y reversals. *J. Geophys. Res.: Space Physics*, *122* (1), 417-431.
 1040 doi:10.1002/2016JA023018
 1041
- 1042 Thomas, E. G. and Shepherd, S. G. (2018). Statistical Patterns of Ionospheric Convection
 1043 Derived From Mid-Latitude, High-Latitude and Polar SuperDARN HF Observations. *J.*
 1044 *Geophys. Res.: Space Physics*, *123* (4), 3196-3216. doi:10.1002/2018JA025280
 1045
- 1046 Tsyganenko, N. A. and Andreeva, V. A. (2015). A forecasting model of the magnetosphere
 1047 driven by an optimal solar wind coupling function. *J. Geophys. Res.*, *120* (10), 8401-8425.
 1048 doi:10.1002/2015JA021641
 1049
- 1050 Volwerk, M., Zhang, T. L., Glassmeier, K. -H., Runov, A., Baumjohann, W., Balogh, A., Rème,
 1051 H., Klecker, B. and Carr, C. (2008). Study of waves in the magnetotail region with cluster and
 1052 DSP. *Advances in Space Research*, *41* (10), 1593-1597. doi:10.1016/j.asr.2007.04.005.
 1053
- 1054 Wei, X. H., Cai, C. L., Cao, J. B., Rème, H., Dandouras, I., and Parks, G. K. (2015). Flapping
 1055 motions of the magnetotail current sheet excited by nonadiabatic ions. *Geophys. Res. Lett.*,
 1056 *42*, 4731-4735. doi:10.1002/2015GL064459
 1057
- 1058 Wei, Y. Y., Huang, S. Y., Rong, Z. J., Yuan, Z. G., Jiang, K., Deng, X. H., Zhou, M., Fu, H. S., Yu,
 1059 X. D., Xu, S. B., He, L. H. and Deng, D. (2019). Observations of Short-period Current Sheet
 1060 Flapping Events in the Earth's Magnetotail. *The Astrophysical Journal Letters*, *874*, 7pp.
 1061 doi:10.3847/2041-8213/ab0f28/pdf.
 1062
- 1063 Wu, M., Lu, Q., Volwerk, M., Vörös, Z., Ma, X., and Wang, S. (2016). Current sheet flapping
 1064 motions in the tailward flow of magnetic reconnection. *J. Geophys. Res.*, *121* (8), 7817-7827.
 1065 doi:10.1002/2016JA022819
 1066



1067 Zhang, L. Q., Baumjohann, W., Wang, C., Dai, L., and Tang, B. B. (2016). Bursty bulk flows at
1068 different magnetospheric activity levels: Dependence of IMF conditions. *J. Geophys. Res.*,
1069 121 (9), 8773-8789. doi:10.1002/2016JA022397
1070
1071